J. Fluid Mech. (1998), *vol.* 357, *pp.* 59–81. Printed in the United Kingdom

Effects of surface film on the linear stability of an air–sea interface

By ØYVIND SAETRA†
Department of Geophysics, University of Oslo, PO Box 1022, Blindern, 0315 Oslo, Norway

(Received 28 February 1996 and in revised form 6 October 1997)

The linear stability of turbulent shear flow over a film-covered sea surface is studied theoretically. A compound matrix method (Wheless & Csanady 1993), is used to solve the eigenvalue problem numerically. The numerical method has been adjusted to a coupled air–sea system. In the stability problem the vertical component of the turbulent Reynolds stress has been taken into account. As pointed out by Wheless & Csanady, the second derivative of the traditional log–linear wind profile has a rather extreme behaviour near the matching point of the linear and logarithmic part. To improve the model, a new profile is calculated based on an eddy viscosity distribution for channel flow (Quarmby & Anand 1969), which has continuous derivatives all the way down to the surface. Calculations of the wave growth rates corresponds well with earlier theoretical results as well as laboratory measurements. The energy flux from the air to the sea caused by the pressure work at the surface has been calculated. An intriguing result obtained here is that this flux seems to be strongly dependent on the elastic property of the surface film. The flux attains a maximum for finite values of the film elasticity parameter.

1. Introduction

The damping effect of oil on waves has been known for at least two thousand years and references may be traced back to Aristotle (Plutarch 95 AD). For people who are dependent on the ocean for fishing and hunting, this effect is well known. One story from the fishing community Hamingberg in northern Norway tells about a life-saving exploit in 1894 where thirty-four lives were saved during a heavy winter storm. The crew of the rescue boat constantly poured cod liver oil around the open fishing vessels to calm the sea so the men could be hauled on board. In antiquity, Mediterranean pearl divers used to release oil from beneath the water. When it rises to the surface, the ripples disappear, which improves the sub-sea light conditions. For further reading the historical review by Scott (1977) is recommended.

The first mathematical model was formulated by Lamb (1932), who calculated the viscous damping rate for two extreme cases: a clean surface and an inextensible surface film, assuming that the upper threshold value would be obtained in the latter case. Dorrestein (1951) showed that this was not so. He calculated the damping rate for general values of the surface elasticity modulus and found that maximum damping occurs for finite values of this parameter. The damping was shown to be exactly twice that obtained for an inextensible film. This effect is related to the existence of longitudinal elastic waves within the film (Lucassen 1982). Maximum damping occurs

† Present address: The Norwegian Meteorological Institute, PO Box 43, Blindern, 0313 Oslo, Norway.

when the frequencies of the transverse capillary–gravity wave and the longitudinal film wave nearly coincide (Dysthe & Rabin 1986).

The introduction of satellite oceanography and radar probing of the ocean surface has renewed the interest in this topic. Oil slicks may be seen as dark patches on radar images because the calming of surface ripples alters the radar backscatter. One severe problem here is how to discriminate between petroleum spill and the naturally formed surface films in the ocean.

The earliest mechanism suggested for wind generation of waves was the classical Kelvin–Helmholz instability. This is modelled by uniform flows in the air and the water, the flows being discontinues at the interface. Owing to the large difference in density between air and water, this mechanism is unable to produce waves for wind speeds below $6.8\,\mathrm{m\,s^{-1}}$. Since waves are found at wind speeds below $1\,\mathrm{m\,s^{-1}}$, other mechanisms obviously must be involved. Miles (1957*a*) successfully explained wave generation for low wind speeds by calculating the growth rate for surface waves due to shear instability of the air flow. He found the growth rate to be proportional to $|U_c''|/|U_c'|^3$, where U_c'' is the curvature of the wind profile at the point where the wind speed and phase speed coincide (the critical point). Here the inviscid version of the governing equation becomes singular. However, the Miles mechanism is incapable of generating waves in the capillary–gravity regime because, for small wave speeds, the critical point will be confined within the viscous boundary layer where the wind profile is almost linear.

Benjamin (1958) extended Miles' theory by taking the effect of molecular viscosity at the boundary into consideration. Later Miles (1962) also calculated a growth rate for capillary–gravity waves which is in good agreement with results from various numerical calculations. For short waves the main agent for instability seems to be the viscous shear stress at the surface.

The effect of a vertical turbulent Reynolds stress was investigated by Jacobs (1987), van Duin & Janssen (1992) and Miles (1993), utilizing an eddy assumption for the turbulent stresses. In these investigations the effect of velocity curvature on wave generation was neglected. The energy transfer from the air to the sea in this case was shown to be dependent on the vertical gradient of the eddy viscosity. One objective of the present study is to incorporate this effect into a more general model for wave growth.

It is a fact that most wave tank measurements are carried out in closed wind tunnels. Here the measurements of Larson & Wright (1975) are particularly interesting, since microwave backscatter is used for measuring the energy growth rate. This is in principle the same technique as used in satellite oceanography for detection of surface films. The present model is well adopted to conditions that occur in wind tunnels. This is particularly so for the way we define our wind profile.

Taking one step at a time, a very simple model of the surface film is used. The effects of solubility of the film material are entirely neglected, and the only parameter regarded as important is the surface elasticity. This is believed to give at least a crude estimate of the effect of surface films on the growth conditions for wind waves. Creamer & Wright (1992) calculated the growth rate by using the Ricatti method which is a different (but related) numerical technique for solving stiff differential equations. By disregarding the turbulent Reynolds stress, and using a log–linear profile, the results obtained with our compound matrix method are shown to be identical to those of Creamer & Wright.

2. Mathematical formulation

2.1. *Equations of motion*

Both air and water are taken to be incompressible homogenous viscous fluids. A Cartesian coordinate system is chosen with the z-axis positive upwards. The (x, y)-axes are situated at the undisturbed surface, and the basic flow and the wave propagation are both in the positive x-direction. The motion occurs in the (x, z)-plane, and the solutions are taken to be periodic in x. The governing equations for air and water are

$$\frac{\mathrm{D}\boldsymbol{u}_{a,w}}{\mathrm{d}t} = -\frac{1}{\rho_{a,w}}\boldsymbol{\nabla} p_{a,w} + \boldsymbol{\nabla}\cdot(\nu_{a,w}(\boldsymbol{\nabla}\boldsymbol{u}_{a,w} + (\boldsymbol{\nabla}\boldsymbol{u}_{a,w})^T)), \tag{1}$$

$$\boldsymbol{\nabla}\cdot\boldsymbol{u}_{a,w} = 0. \tag{2}$$

Here $\boldsymbol{u} = (u, w)$ is the velocity, $\mathrm{D}/\mathrm{d}t$ is the material derivative, T denotes the transpose and the subscripts a and w indicate the air and water, respectively. The constant fluid density is ρ, and p is the dynamic pressure. The kinematic viscosity coefficient for air is traditionally written as (Jacobs 1987; van Duin & Janssen 1992; Miles 1993)

$$\nu_a = \nu_o + \nu_e(z), \tag{3}$$

where ν_o is the constant molecular value, and $\nu_e(z)$ is the turbulent eddy viscosity which is assumed to vary with z only. For water, ν_w is taken to be constant.

Perturbing the basic flow $U(z)$, and assuming small disturbances u, w, p so the equations can be linearized, the system of equations for the perturbed problem now becomes

$$\frac{\partial u}{\partial t} + U\frac{\partial u}{\partial x} + U'w + \frac{1}{\rho}\frac{\partial p}{\partial x} = \nu\nabla^2 u + \nu'\left(\frac{\partial u}{\partial z} + \frac{\partial w}{\partial x}\right), \tag{4}$$

$$\frac{\partial w}{\partial t} + U\frac{\partial w}{\partial x} + \frac{1}{\rho}\frac{\partial p}{\partial z} = \nu\nabla^2 w + 2\nu\frac{\partial w}{\partial z}, \tag{5}$$

$$\frac{\partial u}{\partial x} + \frac{\partial w}{\partial z} = 0. \tag{6}$$

Here the primes denote the differentiation with respect to z. In these equations the subscripts a and w have been deleted since the equations are valid for both air and water. Since the motion is two-dimensional and incompressible, we may introduce a stream function ψ such that

$$u = \frac{\partial \psi}{\partial z} \quad \text{and} \quad w = -\frac{\partial \psi}{\partial x}. \tag{7}$$

Applying normal mode decomposition, we write the stream function as

$$\psi = \quad (z)\,\mathrm{e}^{\mathrm{i}k(x-ct)}, \tag{8}$$

where k is a real wavenumber and c is the complex phase velocity. Eliminating the pressure from equations (4) and (5), we obtain a fourth-order equation for the amplitude function:

$$(U-c)(\quad''-k^2\quad)-U''\quad = \frac{\nu}{\mathrm{i}k}(\quad^{\mathrm{iv}}+K_3\quad'''+K_2\quad''+K_1\quad'+K_0\quad), \tag{9}$$

where

$$K_0 = k^2\left(\frac{\nu''}{\nu}+k^2\right), \quad K_1 = -2\frac{\nu'}{\nu}k^2, \quad K_2 = \frac{\nu''}{\nu}-2k^2, \quad K_3 = 2\frac{\nu'}{\nu}. \tag{10}$$

For laminar flow, ν is constant. Equation (9) then reduces to the well-known Orr–Sommerfeld equation.

2.2. *Boundary conditions*

At the surface, the horizontal and vertical velocity components must be continuous. Also, the stress differences across the interface have to be balanced by the stresses within the film. For the basic flow, the kinematic condition at the interface implies that

$$U_a(0) = U_w(0) = U_o, \tag{11}$$

where U_o is the surface drift (assumed to be constant in time). The condition on the horizontal stress gives

$$\rho_a \nu_a U_a'(0) = \rho_w \nu_w U_w'(0). \tag{12}$$

For the total velocity to satisfy the continuity condition at the surface $z = \zeta$, we must require to first order that

$$w_a(0) = w_w(0), \tag{13}$$

$$u_a + \zeta U_a' = u_w + \zeta U_w' \quad \text{for} \quad z = 0. \tag{14}$$

The dynamic boundary condition in the vertical direction states that the difference in normal stress on each side of the surface must be balanced by surface tension, i.e.

$$\mu_w\left(2\frac{\partial}{\partial z}(w_w) - \frac{\partial \zeta}{\partial x}U_w'\right) - p_w + \rho_w g\zeta - \left\{\mu_a\left(2\frac{\partial}{\partial z}(w_a) - \frac{\partial \zeta}{\partial x}U_a'\right) - p_a + \rho_a \zeta\right\} = \sigma\frac{\partial^2 \zeta}{\partial x^2}, \tag{15}$$

where σ is the surface tension and $\mu = \rho\nu$ is the dynamic viscosity. The perturbation pressure may be obtained from (4). Writing the pressure as $p = P(z)\,\mathrm{e}^{\mathrm{i}k(x-ct)}$, we find

$$P = \rho\left[(c-U)\ \ ' + U'\ \ + \frac{\nu}{\mathrm{i}k}\left\{\left(\frac{\mathrm{d}^2}{\mathrm{d}z^2} - k^2\right)\ \ ' + \frac{\nu'}{\nu}\left(\frac{\mathrm{d}^2}{\mathrm{d}z^2} - k^2\right)\ \ \right\}\right]. \tag{16}$$

Within the viscous boundary layer the turbulent Reynolds stresses vanish, and accordingly ν' must be zero at the surface.

Allowing the surface to be contaminated, i.e. covered by a surface film, the difference in tangential stress across the interface must be balanced by the surface tension gradient. In the linear approximation,

$$\mu_w\left(\frac{\partial u_w}{\partial z} + \frac{\partial w_w}{\partial x} + U_w' + \zeta U_w''\right) - \mu_a\left(\frac{\partial u_a}{\partial z} + \frac{\partial w_a}{\partial x} + U_a' + \zeta U_a''\right) = \frac{\partial \sigma}{\partial x}. \tag{17}$$

The surface tension gradient is related to the fluid velocity at the surface by introducing the complex surface dilational modulus E, defined as

$$E = \frac{\partial \sigma}{\partial(\ln(A))}. \tag{18}$$

Here A is the area per molecule of film material (Lucassen 1982). The real part of E represents the film elasticity and the imaginary part describes the phase shift between the areas of maximum surface dilation or compression and the variable part of the surface tension. Assuming linear motion, conservation of film material implies

$$\frac{\partial}{\partial x}\left(\frac{\partial}{\partial t} + U_o\frac{\partial}{\partial x}\right)\sigma = E\left(\frac{\partial^2 u}{\partial x^2} + U'\frac{\partial^2 \zeta}{\partial x^2}\right), \quad z = 0. \tag{19}$$

Now equations (11), (12), (16) and (19) may be used to express the four boundary

conditions (13), (14), (15) and (17) at the surface in terms of the stream function (8). We then obtain the following boundary conditions to be satisfied at $z = 0$:

$$ _a = \ _w, \tag{20}$$

$$\frac{U_a'}{c-U_o}\ _a + \ '_a = \frac{U_w'}{c-U_o}\ _w + \ '_w, \tag{21}$$

$$\frac{\mu_a}{\mu_w}\left[\left(\frac{U_a''}{c-U_o}+k^2\right)\ _a + \ ''_a\right] = \left(\frac{U_w''}{c-U_o}+k^2\right)\ _w + \ ''_w + \frac{\mathrm{i}kE}{(c-U_o)\mu_w}\left(\ '_w + \frac{U_w'}{c-U_o}\ _w\right), \tag{22}$$

$$\frac{\rho_a}{\rho_w}\left[\left(U_a'-\frac{g}{c-U_o}\right)\ _a + (c-U_o+3\mathrm{i}k\nu_a)\ \ '_a + \frac{\nu_a}{\mathrm{i}k}\ \ '''_a\right]$$

$$= \left(U_w'-\frac{g+\sigma k^2/\rho_w}{c-U_o}\right)\ _w + (c-U_o+3\mathrm{i}k\nu_w)\ \ '_w + \frac{\nu_w}{\mathrm{i}k}\ \ '''_w. \tag{23}$$

Far away from the surface we assume that the velocity perturbations vanish. Accordingly, we take

$$, \ ' \to 0 \quad \text{when} \quad |z| \to \infty \tag{24}$$

in both air and water.

In this study we will restrict ourselves to include only real values of E, since for most films with moderate values of the surface dilational viscosity, the real part seems to be the most important parameter for the wave-damping characteristics. The magnitude of the surface elasticity may vary between zero (clean surface) and at least 50 dyn cm^{-1}. Hühnerfuss, Lange & Walter (1985) have measured the surface elasticity for different chemical compounds and have obtained values of more than 80 dyn cm^{-1}. When the wavenumber is of order 1 cm^{-1}, elasticity values of this magnitude will make the terms that include E dominate any other terms in the boundary condition (22).

2.3. *Mean wind profiles*

To model the atmospheric surface layer flow in order to investigate the stability of the air–sea interface, a log–linear profile originally suggested by Miles (1957*b*) has become more or less standard. The basic profile is obtained by matching a profile which is linear in the viscous boundary layer with one which becomes asymptotically logarithmic. The two profiles are matched at the height z_o, which is a measure of the thickness of the viscous boundary layer. It is defined as

$$z_o = \frac{m\nu_o}{u_*}, \tag{25}$$

where u_* is the friction velocity in the air. The parameter m is of order unity, and values vary from five to eight in the literature. The basic wind velocity profile is given as

$$\left.\begin{aligned} U_a &= \frac{u_*^2}{\nu_o}z + U_o, && 0 \leqslant z \leqslant z_o, \\ U_a &= U_o + mu_* + 2.5u_*(\Theta - \tanh\Theta), && z \geqslant z_o, \\ \sinh\Theta &= \frac{0.8u_*}{\nu_o}(z-z_o). \end{aligned}\right\} \tag{26}$$

Wheless & Csanady (1993) report that the compound matrix method could not cope with this wind profile, claiming that this is caused by the near-discontinuity of the

second derivative of the mean velocity U_a'' at the matching point. For this reason, and because the overall behaviour of the log–linear profile is unrealistic near the matching point, they constructed a new mean velocity profile with a small second derivative. This new profile is based on an integrated error-function, and is written

$$U_a = U_\infty - (U_\infty - U_o)\,\pi^{1/2}\,\mathrm{i}\,\mathrm{erfc}\,[bz], \tag{27}$$

where $b = u_*^2/(\pi^{1/2}\nu_a(U_\infty - U_o))$ and U_∞ is the asymptotic value. Note that in this profile the second derivative does not vanish at the surface.

When implementing the compound matrix method, we had no problems with the log–linear profile. As shown later, the method produced results which were in very good agreement with those of Creamer & Wright (1992). The failure of the log–linear profile in the calculations of Wheless & Csanady is therefore not clear to us. However, it is true that the second derivative of the log–linear profile has a rather extreme behaviour when approaching the viscous sublayer. Especially for capillary–gravity waves, which have the critical point in this region, this behaviour is unsatisfactory.

The growth rate values obtained by Wheless & Csanady are much larger than the numerical results obtained with the log–linear profile and they suggest that the cause for this might be the velocity profile differences. If this is true it means that the growth rates are very sensitive to changes in the shape of the wind velocity distribution. To resolve this problem we need to compare with the results from a velocity profile which does not suffer from the unphysical behaviour of the log–linear and the error-function profiles, i.e. it must have a smooth second derivative which approaches zero at the air–water interfaces. For this purpose a wind profile based on the eddy viscosity for channel flow by Quarmby & Anand (1969) has been chosen. This profile is also suitable for comparing with experimental data. here the eddy viscosity is defined as

$$\frac{\nu_e}{\nu_o} = \frac{1.15}{2}\left\{1 + \frac{0.16}{9}\hat{r}_o^2\left[1 - \left(\frac{\hat{r}}{\hat{r}_o}\right)^2\right]^2\left[1 + 2\left(\frac{\hat{r}}{\hat{r}_o}\right)^2\right]^2\left[1 - \exp\left(-\frac{\hat{z}}{26}\right)\right]^2\right\}^{1/2} - \frac{1.15}{2}. \tag{28}$$

Denoting the distance to the centre of the channel by r_o, the non-dimensional parameters in (28) are defined as

$$\hat{r}_o = \frac{r_o u_*}{\nu_o}, \quad \hat{z} = \frac{z u_*}{\nu_o}, \quad \hat{r} = \hat{r}_o - \hat{z}. \tag{29}$$

Using the equation of motion for two-dimensional, stationary channel flow, the wind velocity profile may now be calculated from

$$U_a(z) = u_*^2 \int_0^z [(1 - z/r_o)/(\nu_o + \nu_e)]\,\mathrm{d}z. \tag{30}$$

In figure 1(*a*) the velocity profiles for $u_* = 15$ cm s^{-1} are compared. Figure 1(*b*) is a close-up of the viscous boundary layer, and depicts the behaviour of the second derivative. In the log–linear profile the value of m is 5.5, and in the new profile r_o is 15 cm, corresponding to the size of the wave tank used in the experiments of Larson & Wright (1975).

2.4. *Basic velocity profile in the water*

Assuming constant wind stress at the surface and laminar flow independent of x, the equation of motion for water initially at rest is

$$\nu_w \frac{\partial^2 U_w}{\partial z^2} - \frac{\partial U_w}{\partial t} = 0. \tag{31}$$

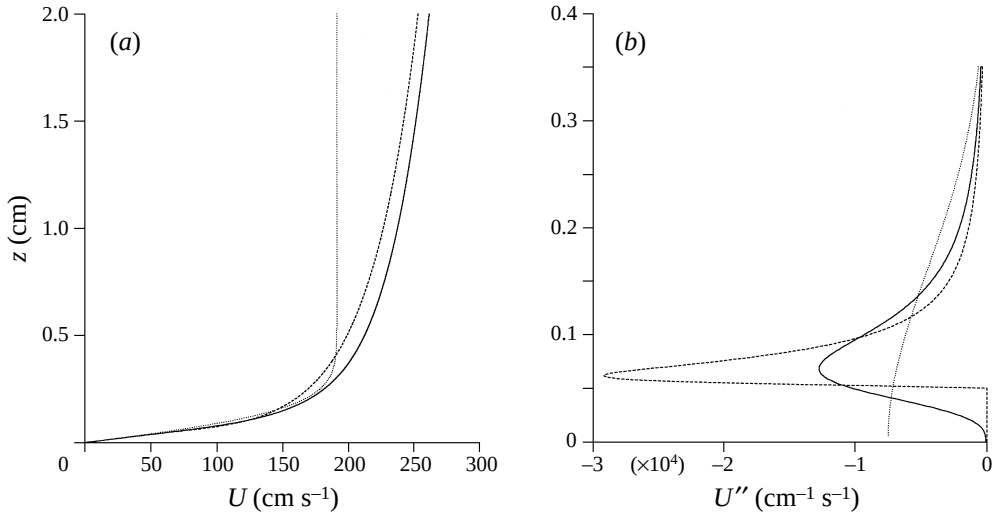

FIGURE 1. Comparison between the channel-flow profile (solid line), error-function profile (dotted line) and the log–linear profile (broken line) for $u_* = 15$ cm s^{-1}. (*b*) is a close up of the second derivative near the air–water surface.

For an infinitely deep ocean the boundary conditions are

$$\frac{\partial U_w}{\partial z} = \frac{\rho_a u_*^2}{\rho_w \nu_w} \quad \text{for} \quad z = 0, \tag{32}$$

$$U_w \to 0 \quad \text{when} \quad z \to -\infty. \tag{33}$$

The initial condition is taken to be

$$U_w = 0 \quad \text{for} \quad t = 0. \tag{34}$$

The solution for U_w may be found by Laplace transforming (31)–(33), utilizing (34). The result is

$$U_w(z, t) = \frac{\rho_a}{\rho_w} \frac{u_*^2}{\nu_w^{1/2}} \int_0^t [\mathrm{e}^{-z^2/(4\nu_w \hat{t})}/(\pi \hat{t})^{1/2}] \, \mathrm{d}\hat{t}. \tag{35}$$

We note that U_w never will tend toward a steady state. However, in our description up to now we have assumed a time-independent basic flow in both air and water. For that reason (35) must be used as a quasi-stationary function at a fixed time point, say a few seconds after the onset of the wind stress. We realize of course that by including the Coriolis force, a steady Ekman flow will develop in the water. However, the time scales considered here are much smaller than the inertial period, so we can safely neglect the effect of the Earth's rotation.

If (35) is used when solving the stability problem numerically, both the profile and its derivatives must be calculated by numerical integration at each grid point. This will make the program extremely time consuming. For this reason, and because we assume that the exact form of the water profile is of secondary importance in this problem, (35) will only be used for calculation of the surface drift U_o. When calculating the eigenvalues, a very simple basic water velocity distribution, starting with U_o at the surface and decaying exponentially, will be used, i.e.

$$U_w = U_o \exp(2z/L_s). \tag{36}$$

Here $L_s = 2(\nu_w t)^{1/2}$ is the viscous boundary layer thickness after t s. This is the same expression for U_w as suggested by Wheless & Csanady (1993).

3. Numerical method

For large Reynolds numbers the physical problem will be dominated by two distinct length scales. This makes (9) a so-called stiff differential equation. When trying to solve this as an initial-value problem with a standard shooting method, the solution will be contaminated by the rapidly growing viscous solution. This will lead to parasitic growth (Drazin & Reid 1981). To overcome this problem a compound matrix method as suggested by Ng & Reid (1979) has been used. The idea is to do a nonlinear transformation of the eigenvalue problem based on the 2×2 minors of a solution matrix.

After an initial guess for the eigenvalue c is implemented, an iterative method is used to vary the eigenvalue till the boundary conditions are satisfied. The calculations were interrupted when the relative error was less than 10^{-8}. The starting distance from the surface was varied in the calculations until no change in the eigenvalue was observed. Taking ν_o/u_* as a measure of the viscous layer thickness, a distance of 200 times this quantity was usually sufficiently far from the surface for starting the calculations. This interval was divided into 2000 steps in both air and water. A detailed description of how the compound matrix method is adapted to a wavy boundary problem is given in the Appendix.

4. Results obtained with a constant viscosity

Before the effect of a variable turbulent eddy viscosity was included, it was decided to test the ability of the numerical program to reproduce results from earlier studies, and to sort out how important details of the wind velocity distribution are for the resulting growth rate. The most commonly used air velocity profile is the log–linear profile (26). This is the one also used by Creamer & Wright (1992), who solve the problem numerically with a Ricatti method. As mentioned before, Wheless & Csanady (1993) failed to incorporate this profile in the compound matrix method, and claim that this is caused by the near-discontinuity in its second derivative. This is peculiar, because the second derivative of the log–linear profile is actually not discontinuous. The second derivative does have a corner point at the matching point z_o, which means that the third derivative is discontinuous here, but the third derivative does not appear equation (9). Furthermore, why does the Ricatti method manage to overcome this problem while the compound matrix method according to Wheless & Csanady fails?

We found this question intriguing, and decided to give the log–linear profile a second try. The outcome was that this profile gave no problems whatsoever, and it even produced results which are in good agreement with those of Creamer & Wright. Figure 2(*a*) shows the results for the film-free case with four different values of the friction velocity u_*: 13.6, 16.9, 21.3 and 24.8 cm s^{-1}. The surface drift velocity is 7.5, 9.6, 9.8 and 10.2 cm s^{-1}, respectively. Here the growth rate is defined as

$$\beta = 2k \operatorname{Im} c. \tag{37}$$

The values of the parameters are $g = 980.1$ g s^{-2}, $\sigma = 72$ dyn cm^{-1}, $\nu_w = 10^{-2}$ cm^2 s^{-1}, $\nu_a = 0.15$ cm^2 s^{-1}, $\rho_w = 1$ g s^{-2} cm^{-1} and $\rho_a = 1.2\ 10^{-3}$ g s^{-2} cm^{-1}. These values correspond to those used by Creamer & Wright in producing figure 4 of their paper. As far as we are able to judge, the results are identical.

Figure 2(*b*) shows the results for $u_* = 24.8$ cm s^{-1} for the film-free case together with the inextensible film case ($E \to \infty$), and the cases $E = 5$ dyn cm^{-1} and $E = 20$ dyn cm^{-1}. These values are the same as those used to produce figure 5(*a*) in Creamer & Wright

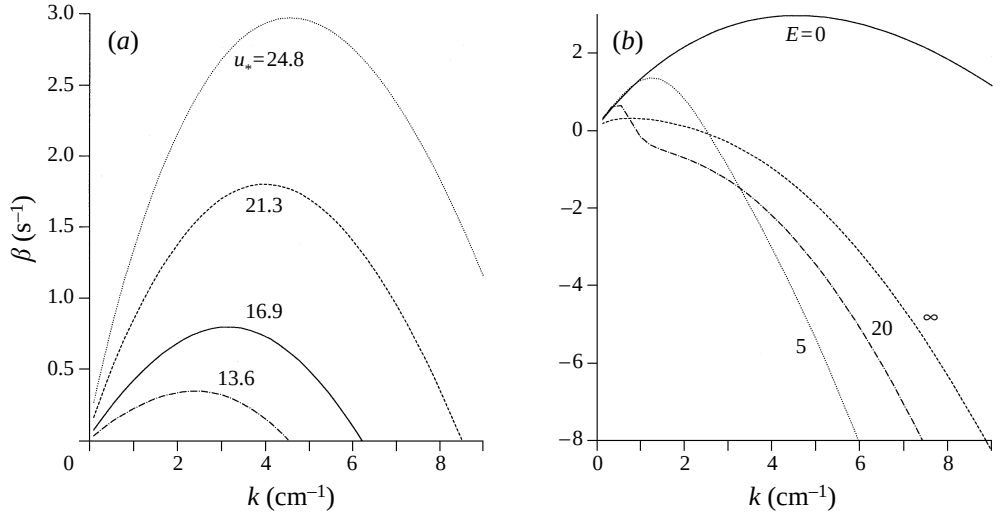

FIGURE 2. Growth rate calculated by use of the log–linear wind-velocity profile (28). (*a*) $E = 0$ and various values of u_* in cm s^{-1}; (*b*) $u_* = 24.8$ and various values of E in dyn cm^{-1}.

(1992). Also in this case the results are almost identical to those of Creamer & Wright. The conclusion so far is that the compound matrix method is fully capable of handling the log–linear profile.

In figure 2(*b*), the graph for $E = 20$ dyn cm^{-1} has a sharp peak and an inflection point which is not found in the others. The explanation for this is probably the so-called Marangoni effect which for a finite elasticity value gives a maximum in the damping ratio for a finite wavenumber. This maximum in damping ratio is more pronounced and is shifted toward longer waves when the film elasticity is increased. For $E = 20$ dyn cm^{-1} the maximum appears as a sharp peak with maximum near $k = 1$ cm^{-1} with a particularly strong damping in the wavenumber band between $k = 0.5$ and 1.5 cm^{-1}, which coincides well with where the growth rate for $E =$ 20 dyn cm^{-1} suddenly drops. For $E = 5$ dyn cm^{-1} the damping ratio has a maximum for $k = 4$ cm^{-1}, but this maximum is much weaker and does not appear as such a sharp peak in a narrow band of the wavenumber space. near $k = 3$ cm^{-1} the damping for $E = 5$ dyn cm^{-1} exceeds the damping for $E = 20$ dyn cm^{-1} which is close to where the growth rate curves for these elasticity values cross (for details on wave damping and surface films, see Herr & Williams 1986).

The relatively high growth rate values obtained by Wheless & Csanady seem to somewhat be confirmed by the experimental results of Larson & Wright (1975). In their figure 12 Wheless & Csanady compared the results for $u_* = 15$ cm s^{-1}, together with the numerical results of Kawai (1979) for $u_* = 17$ cm s^{-1}. From this plot, which is reproduced in figure 3(*a*) of the present paper, their numerical results appear to be in rather good agreement with the measurements of Larson & Wright, while the growth rates calculated by Kawai are far too low. However, this agreement seems to be false: the results of Larson & Wright which are energy growth rate values, $2kc_i$ are compared with the amplitude growth rate values, kc_i, of Kawai and Larson & Wright. Figure 3(*b*) shows the adjusted curves expressed as amplitude growth rates.

The growth rate values calculated by Wheless & Csanady are almost a factor of four larger than the results obtained Kawai (1979) and Creamer & Wright. Also, van Gastel, Janssen & Komen (1985) who solved the instability problem by asymptotic methods found that changes in the shape of the wind profile can change the growth rate

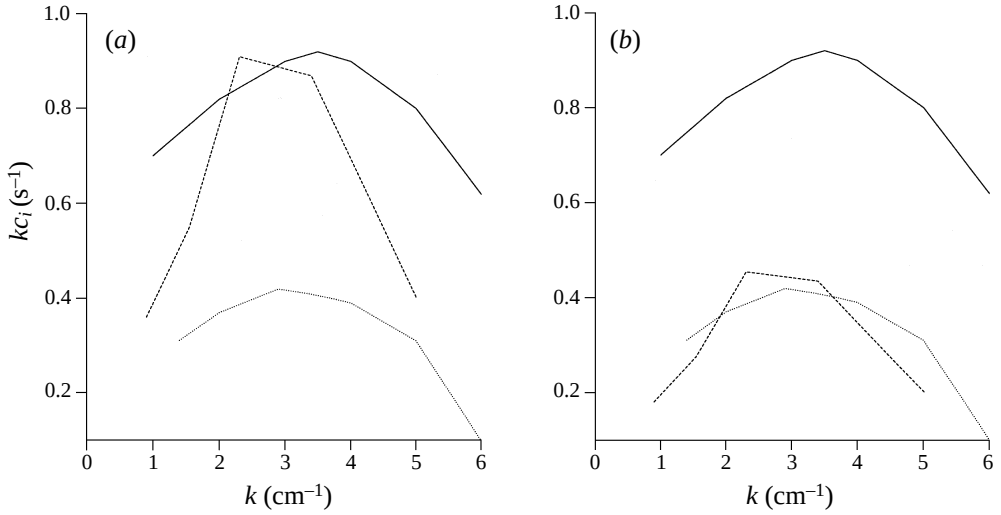

FIGURE 3. (*a*) Figure 12 from Wheless & Csanady. The numerical results obtained by them (solid line) are compared to the measurements of Larson & Wright (broken line) and the numerical results of Kawai (dotted line) for $u_* = 15$ cm s^{-1}. (*b*) The adjusted curves when the results from Larson & Wright are expressed as kc_i.

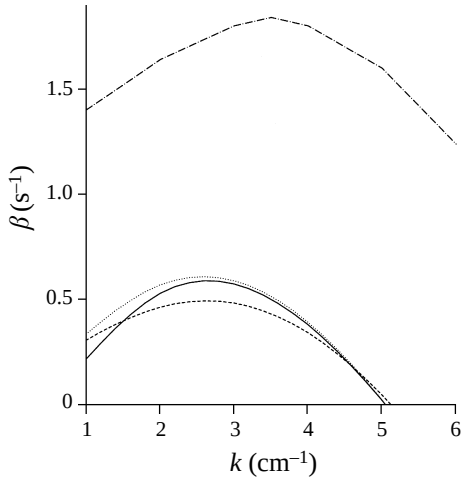

FIGURE 4. The result from using the integrated error-function profile in this study (solid line) compared to the results of Wheless & Csanady (broken-dotted line), the channel-flow profile (dotted line) and the log–linear profile (broken line). The friction velocity is 15 cm s^{-1}.

by a factor of more than three. But in their study the estimate was based on a comparison with a wind profile that is linear outside the viscous boundary layer. To see how sensitive the growth rate is to the exact shape of the wind profile, comparison will be made with the three profiles described in §2.3, which all have a more realistic behaviour outside the viscous boundary layer.

In figure 4 the results of this study using the integrated error-function profile (27), the log–linear profile (26) and the new profile given by (30) are compared with earlier results. When applying (30) to produce this plot, the eddy viscosity was only used when calculating the basic velocity profile. In the equations the molecular values were inserted for the viscosities. here $u_* = 15$ cm s^{-1}, $\sigma = 75$ dyn cm^{-1} and $U_o = 6.8$ cm s^{-1}.

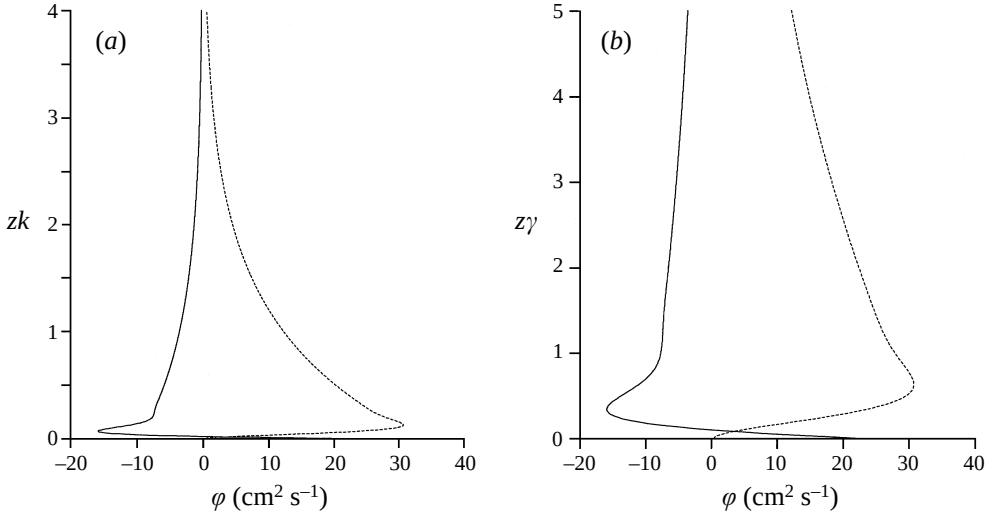

FIGURE 5. Real (solid line) and imaginary (broken line) parts of eigenfunctions. Vertical axis is scaled with wavenumber k in (a), and with the inverse viscous boundary layer thickness γ in (b). The wavenumber is 3 cm^{-1}.

The other parameters are unchanged. As can be seen, the results are quite different from those of Wheless & Csanady. The differences produced by the various wind distributions are about 23%. It is also worth noting that the program has been tested with a velocity profile which grows linearly outside the viscous boundary layer, and it produced results similar to those of van Gastel *et al.* Since the results of Wheless & Csanady are very far from both the other numerical studies and the laboratory study of Larson & Wright, it is most likely that the calculations of Wheless & Csanady are erroneous.

So far comparison with previous results have been done only for the friction velocity 15.0 cm s^{-1}. The results have also been compared for $u_* = 18.0$, 21.0 and 24.0 cm s^{-1}, and are qualitatively the same.

From the present study it may be seen that the growth rate is not strongly sensitive to changes in the shape of the basic velocity profile. The differences produced by the various wind velocity profiles was about 23%. This result is quite encouraging, especially since our knowledge of the wind profile in a real situation is rather poor. These results may indicate that a simple velocity profile like the log–linear one, gives an adequate representation of constant wind distribution with height over open water as far as growth rates are concerned.

In figure 5(a) the real and imaginary parts of the eigenfunction for $u_* = 24.0$ cm s^{-1} are shown. To demonstrate the exponential decay of the form e^{-kz}, the vertical axis is scaled with the wavenumber which is equal to 3 cm^{-1} in this case. Figure 5(b) is a close up of the rapid variation close to the boundary, and is scaled with the viscous boundary layer thickness

$$\gamma = (\omega/2\nu_a)^{1/2}. \tag{38}$$

5. Effect of a variable eddy viscosity

As mentioned earlier, the effect of an eddy viscosity which is increasing with height has been studied by among others Jacobs (1987), and van Duin & Janssen (1992). In both papers analytic solutions to the instability problem are found. To achieve that, the

effect of molecular viscosity and curvature of the basic wind profile on the wave generation are neglected. In the study by Jacobs the model for the eddy viscosity is taken to be

$$\nu_e = \kappa u_* z, \tag{39}$$

where κ is von Kármán's constant. Van Duin & Janssen considered a family of closure models which includes (39). It is important to note that when used in a logarithmic velocity profile, these closure models will all give the same basic eddy viscosity as (39), with a linear growth with height. In the study by van Duin & Janssen, the effect of different closure models on the growth rate enters only through the perturbation eddy viscosity, and in this way modifies the result given earlier by Jacobs. For moderate wind speed the effect of a variable eddy viscosity is the only mechanism capable of generating waves in this model.

To test the ability of this approach to reproduce earlier results, the model has been modified to resemble the one given by Jacobs (1987) as much as possible. When calculating the boundary condition, the velocity profile in the air is then kept at a constant value everywhere except at $z = 0$, where the velocity is zero. As in the paper by Jacobs, the velocity value $1/k$ above the interface has been used. This is calculated from the logarithmic formula

$$U_a = \frac{u_*}{\kappa} \log\left(\frac{z}{z_o}\right). \tag{40}$$

For the eddy viscosity, equation (39) has been used. The result by Jacobs is

$$2kC_i = 2k\varepsilon\kappa s C_r \left(\frac{V - C_r}{V}\right)\left(\frac{V}{C_r}\right)^2, \tag{41}$$

where $s = \rho_a/\rho_w$ and C_i, C_r are the imaginary and real parts of the complex phase speed, respectively. These must be distinguished from c defined in §2 since here the dissipation in water has not been taken into account and the result is only valid for the rate of pressure work done at the surface, divided by energy density of the waves. Furthermore, V is the wind speed at distance $1/k$ above the surface and $\varepsilon = u_*/V$ which corresponds to the square root of the drag coefficient. Now, since our model includes the dissipation of energy in the water, the program will be run twice, first with the linearly growing eddy viscosity, and then with the varying eddy viscosity switched off. The latter case resembles the classical Kelvin–Helmholz model except for the inclusion of molecular viscosity, and is not expected to give rise to any flux of energy from the air to the water at these wind speeds ($V < 6.8\ \mathrm{m\ s^{-1}}$). By calculating the difference in growth/damping rate in these two cases, the flux from the air to the sea at the surface caused by the linearly growing eddy viscosity should be obtained. The result is shown in figure 6 together with the result obtained from (41). One must remember that this method is not identical to the model described by Jacobs. This case, for instance, also includes viscous dissipation of energy in the air. With this taken into account, it seems as the main features of the result given by (41) is well reproduced with this approach.

When deriving equation (9) the wave-induced perturbation eddy viscosity was not included. Also, the formula obtained by Jacobs may be found without considering this part of the eddy viscosity. Actually, this will lead to a discontinuity in the pressure across the outer and inner layers. However, it can be shown that, if the mean eddy viscosity is taken into account, the pressure at the surface can be obtained from the outer-layer pressure by letting $z \to 0$. Van Duin & Janssen included the perturbation

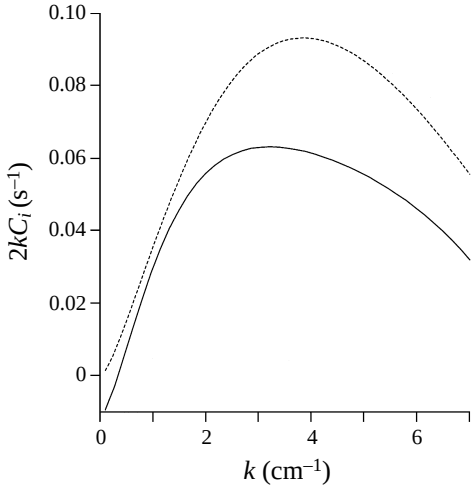

FIGURE 6. Results obtained by the formula from Jacobs (broken line) compared to the results obtained numerically (solid line) with a velocity profile which is constant with height. The friction velocity here is 15 cm s^{-1}.

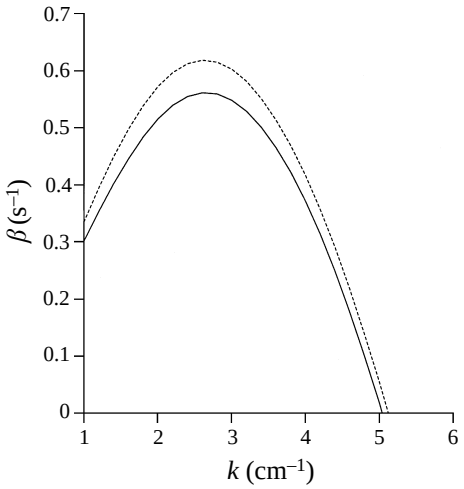

FIGURE 7. Growth rate calculated by use of the channel-flow profile (33) and variable eddy viscosity (solid line) compared to the results obtained with a constant viscosity (broken line). The friction velocity is 15 cm s^{-1}.

eddy viscosity in their study: they obtained the same formula as Jacobs (41), but with a small additional correction term caused by the perturbation viscosity. Since the perturbation eddy viscosity is unknown, an assumption has to be made on how it should be related to the mean velocity field. Therefore, to avoid introducing one more uncertain assumption, the perturbation eddy viscosity will not be taken into account in this paper.

The results are shown for $u_* = 15$ cm s^{-1}. However, qualitatively the results are the same for other values of the friction velocity. The velocity profile is taken to be the channel-flow profile (30). Figure 7 shows the growth rate when the effect of a turbulent eddy viscosity is included. The eddy viscosity is calculated from (28) and the results are compared with those obtained from the same model with only the molecular value for

the viscosity. As can be seen, the growth rate obtained with a constant viscosity exceeds the result when a varying eddy viscosity is included. Based on the results obtained by Jacobs and by van Duin & Janssen, the inclusion of a variable eddy viscosity was expected to increase the resulting growth rate by approximately the same order of magnitude as the values obtained in those studies. The surprising result here is that when the effect of a variable eddy viscosity is included in a model which also includes curvature of the wind profile and the dynamics of the viscous boundary layer, the basic eddy viscosity term will slightly reduce the wave growth. Miles (1993) calculated the energy transfer in a model which included contributions from both the curvature of the wind profile and variable eddy viscosity, but the contributions were calculated independently by neglecting the critical-layer component when calculating the eddy viscosity component and vice versa. This resulted in two terms in the growth rate formula: one eddy viscosity component, equal to the Jacobs formula, and one critical-layer component. If the results obtained in this study are correct, it may indicate that an approach where effects such as the curvature of the velocity profile and molecular viscosity are neglected is too idealized to adequately model the effect of a variable eddy viscosity on the initial growth of short waves in moderate wind conditions. The results by Jacobs disagree with the present study on whether this effect enhances or restrains wave growth, but in both studies the magnitude of this effect is small. The main contribution to the wave growth for short waves in the capillary–gravity regime, for which the critical layer is inside the viscous boundary layer, seems to arise from the dynamics of this viscous sublayer itself. This is also in accordance with the conclusions by several earlier authors, e.g. Phillips (1977).

6. Energy flux

The energy transfer from the air to the sea is calculated from the work done at the surface by the pressure part in phase with the wave slope, divided by the energy density of the waves, $\Omega = \zeta_0^2(\rho_w g + \sigma k^2)/2$. The energy flux is

$$F = P_{i\ \ r}/\Omega, \tag{42}$$

where i denotes the imaginary and r the real part. Since both pressure and eigenfunctions are proportional to ζ_o the amplitude will cancel in (42). In figure 8(*a*) the result for the energy flux vs. film elasticity for a fixed wavenumber ($k = 3\ \mathrm{cm}^{-1}$) is shown. Here four different values of u_* have been used. A striking feature is the maximum in energy transfer for finite values of the elasticity modulus, near $E \approx 5\ \mathrm{dyn\ cm}^{-1}$, which shows how the flux is dependent on the elastic properties of the film. It is interesting to compare this behaviour with the maximum damping obtained for finite values of the film elasticity in the absence of wind. The damping is given by

$$\beta_{int} = -\frac{k\omega}{4\gamma}\left(\frac{2\alpha^2}{1-2\alpha+2\alpha^2} + \frac{k}{\gamma}\frac{4(1-\alpha)}{(1-2\alpha+2\alpha^2)}\right), \tag{43}$$

where

$$\alpha = \frac{\gamma k^2 E}{\rho_w \omega^2} \tag{44}$$

is a non-dimensional elasticity parameter, see Weber & Saetra (1995), and γ is given by (38). For a fixed wavenumber the result (43) yields a maximum for a finite value of the film elasticity parameter. Here α is constructed in such a way that this maximum is attained when $\alpha = 1$. When maximum damping occurs the frequency of the elastic film wave (Marangoni wave) is almost equal to the frequency of the transverse wave.

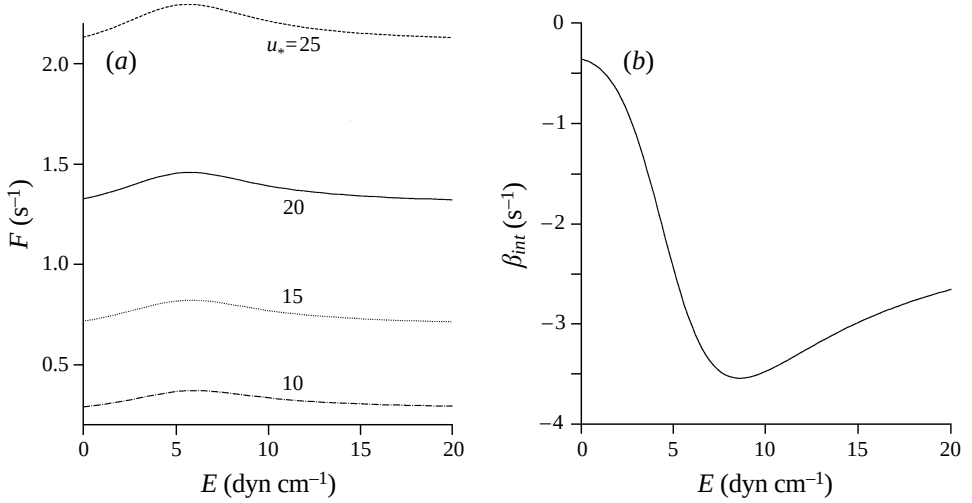

FIGURE 8. The part of the growth rate caused by the external stresses for various u_* in cm s^{-1} (*a*) and the part caused by dissipation of energy in the water phase (*b*) vs. film elasticity. Here $k = 3$.

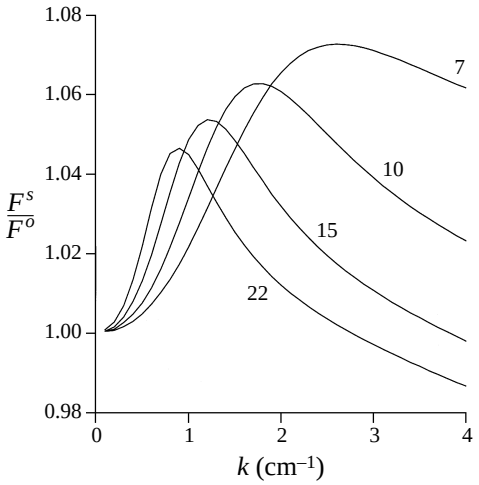

FIGURE 9. Ratio of the flux with a surface film to the flux in the film-free case. The numbers are elasticity values in dyn cm^{-1}.

Whether this maximum in energy transfer is in any way related to the Marangoni wave is not yet clear. In figure 8(*b*) β_{int} vs. film elasticity for $k = 3$ cm^{-1} calculated from (43) is shown. As can be seen the maximum in energy transfer occurs for smaller elasticity values than the maximum in damping.

A maximum in energy transfer for a finite surface elasticity implies that in the case of a surface film with low concentration of surfactant, the conditions for wave growth are improved compared to a clean surface. However, in most cases the enhanced damping caused by the film will dominate this effect and prevent the waves from growing.

In figure 9 the ratio of the flux with a surface film, denoted by F^s, to the flux in the film-free case, denoted by F^o, has been plotted as a function of wavenumber for four

different values of the film elasticity. Again the friction velocity is 15 cm s^{-1}. Like the maximum in damping according to (43), the maximum in energy flux is also shifted towards low wavenumbers when the film elasticity is increased.

7. Comparison with laboratory studies

Measurements of growth rate for wind-generated waves in a wave tank has been carried out by various authors. For the case with no surface film, extensive measurements of initial wave growth the first few seconds after the onset of the wind have been carried out by Larson & Wright (1975), using a microwave backscatter technic. This is in principle the same as the one used in satellite oceanography. In the case with a surface film of sodium lauryl sulphate solution the growth rate has been measured by Gottifredi & Jameson (1970). By measuring the surface tension as a function of concentration, the film elasticity was calculated from an expression equivalent to (18). The effect of both artificial and naturally formed surface slicks on radar backscatter in a real ocean and in wave a tank have been investigated by Hühnerfuss and co-workers (see for instance Alpers & Hühnerfuss 1989). In these papers fully developed wave spectra are considered, and comparison with a model for initial wave growth would probably be rather dubious at the present stage.

In figures 10(*a*) and 10(*b*) the measured growth rate values of Larson & Wright for friction velocity values of 15 and 21 cm s^{-1} are compared with the theoretical results obtained from the channel-flow profile with a variable eddy viscosity and log–linear profile with a constant viscosity. For these moderate wind-velocities the theoretical values seem to be in fairly good agreement with the results from the wave-tank experiments. For stronger winds on the other hand, the theoretical approach seems to fail completely. In figures 11(*a*) and 11(*b*) the theoretical results for friction velocities of 66 and 125 cm s^{-1} are compared to the values obtained in the experiment of Larson & Wright. As can be seen, the growth rate figures calculated from the stability problem exceed the values obtained in a wave tank by several orders of magnitudes.

Donelan & Pierson (1987) have pointed out that the friction velocities quoted by Larson & Wright are too large and they claim that this is because they were measured at steady state after the spectrum had attained its fetch limit. Another explanation for these high friction velocities may be found in the way they were calculated from the wind velocity profile. Larson & Wright calculated the friction velocities from the slope of the measured wind velocity profile plotted with logarithmic values on the z-axis, in accordance with the assumption that the profile has a logarithmic distribution over all the part which is used for calculating the friction velocity values. Since the air flow in a wind tunnel is of a turbulent Poiseuille type, the error introduced by using this method for calculating the friction velocities will probably be most pronounced for the cases of large wind speeds, since then the core region will occupy a greater part of the flow section.

If the continuous velocity distribution is known, the friction velocity may be calculated from the relation

$$U_m - U_a = F(U, u_*, z) = 0, \tag{45}$$

where U_m is the measured wind velocity at the elevation z from the surface, and U_a is the theoretical velocity distribution. Now if we follow this idea, a better friction velocity value should be obtained with the use of equation (30) for U_a in (45) instead of a pure logarithmic distribution. When this method is applied to the wind velocity measurements plotted in figure 11 in the paper by Larson & Wright the result is almost

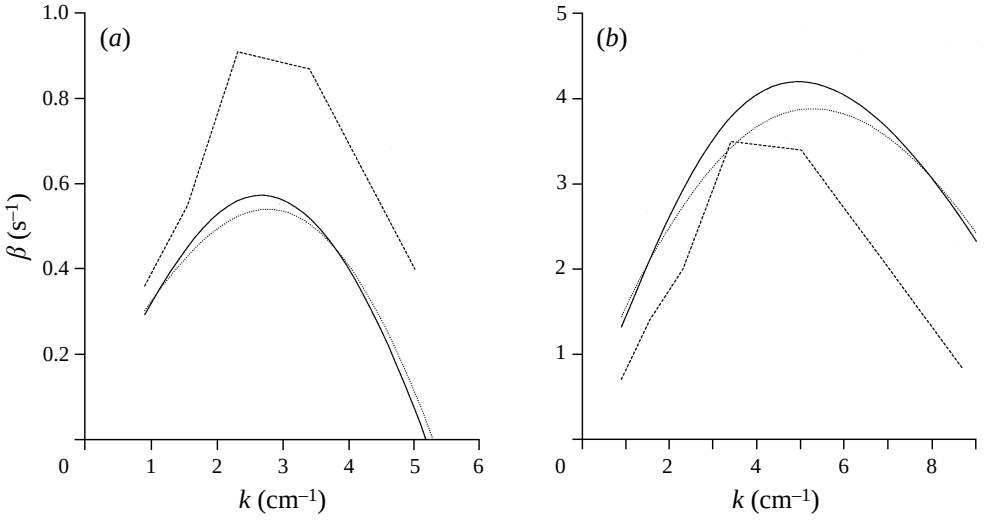

FIGURE 10. Growth rate in the film-free case calculated with the channel-flow profile (solid line) and the log–linear profile (dotted line) compared to the measurements of Larson & Wright (broken line) for friction velocities of (*a*) 15 and (*b*) 27 cm s^{-1}.

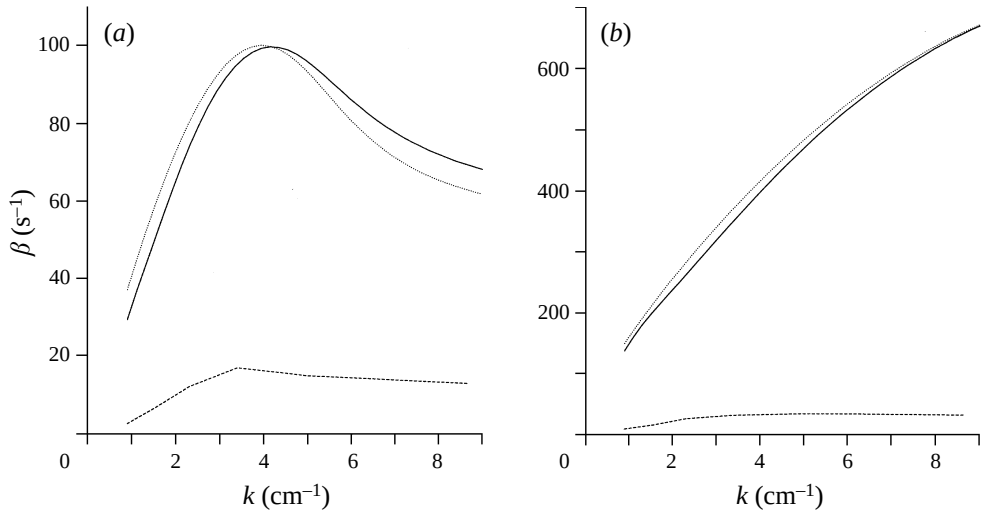

FIGURE 11. As figure 10 but for friction velocities of (*a*) 66 and (*b*) 125 cm s^{-1}.

the same for the two cases of low wind speed: for $u_* = 15$ cm s^{-1} this method yields the same result and where Larson & Wright report a friction velocity of 27 cm s^{-1} the result with this method is approximately 22 cm s^{-1}. Although the result is somewhat lower in the last case, the difference is not more than what could be caused by errors when trying to extract the velocity values from figure 11 in Larson & Wright. Really significant differences are first obtained when we proceed to the two cases with large wind velocity values. In table 1(*a*) the friction velocities calculated at different elevations from the surface with the new method are listed together with corresponding wind speeds for the case where the slope method yields a friction velocity of 66 cm s^{-1}. The mean value obtained with this method is a friction velocity of 38 cm s^{-1}. Table 1(*b*) shows similar

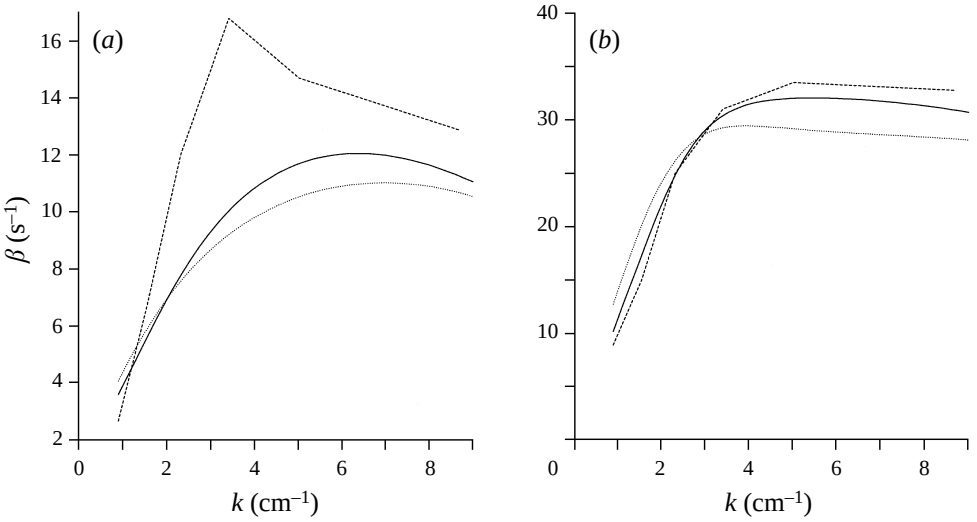

FIGURE 12. Growth rate in the film-free case calculated with the channel-flow profile (solid line) and the log–linear profile (dotted line) compared to the measurements of Larson & Wright with adjusted friction velocity values according to equation (45). In (*a*) and (*b*) the friction velocities are 38 and 52 cm s^{-1}, respectively.

(*a*)							
z (cm)	1.1	1.3	1.5	2.0	2.4	3.0	4.0
U (cm s^{-1})	620	650	675	715	740	760	800
u_* (cm s^{-1})	34.7	35.5	36.2	36.9	37.2	37.2	37.7
z (cm)	5.7	7.2	9.0	10.1	12.1	14.0	
U (cm s^{-1})	845	900	930	950	975	970	
u_* (cm s^{-1})	38.1	39.2	39.4	39.7	40.0	39.5	
(*b*)							
z (cm)	3.1	3.6	4.1	5.2	6.3	8.1	10.2
U (cm s^{-1})	985	1025	1070	1125	1190	1275	1350
u_* (cm s^{-1})	46.9	47.8	49.0	50.0	51.4	53.3	54.8
z (cm)	11.7	13.0	15.0				
U (cm s^{-1})	1405	1430	1450				
u_* (cm s^{-1})	56.2	56.7	57.1				

TABLE 1. Friction velocity values calculated from (45) in the cases where the slope method yields a friction velocity of (*a*) 66 cm s^{-1}, (*b*) 125 cm s^{-1}.

results for the case where the slope method yields $u_* = 125$ cm s^{-1}. The mean value obtained in this case is a friction velocity value of 52 cm s^{-1}.

In figures 12(*a*) and 12(*b*) the theoretical results obtained with the adjusted friction velocity values are plotted together with the measurements. In these cases the growth rate figures calculated with the reduced friction velocity values are in good agreement with the results obtained in a wave tank.

In figure 13 the results from this study are compared to measurements of Gottifredi & Jameson (1970). Here the waves were generated mechanically, and then subjected to the wind. The plot shows the growth rate as a function of friction velocity for a constant wave frequency, 6.20 Hz. The wavenumber has been calculated from equation (2.10) in Gottifredi & Jameson. The symbols refer to two different solutions with

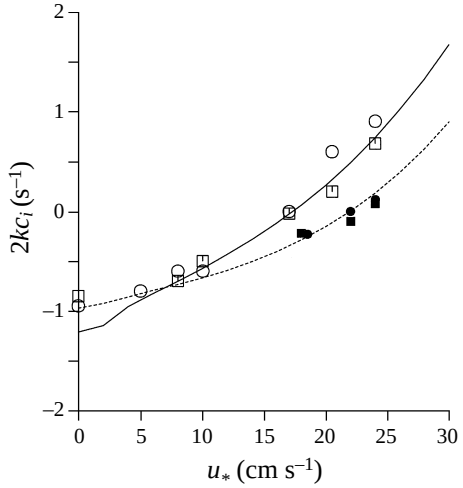

FIGURE 13. Growth rate values for $E = 37$ (broken line) and $E = 15$ dyn cm^{-1} (solid line) as a function of friction velocity compared to the measurements of Gottifredi & Jameson (1970). The frequency is 6.20 Hz. See text for a description of the symbols.

surface tension σ of 58 dyn cm^{-1} (circles) and 34 dyn cm^{-1} (squares), respectively. The open symbols are measurements taken 46 cm from the wavemaker, while the solid symbols are taken 106 cm from the wavemaker. The surface elasticity E is reported to vary between 15 and 37 dyn cm^{-1}. The solid line shows the theoretical results with 15 dyn cm^{-1} for the surface elasticity and 58 dyn cm^{-1} for the surface tension, and the broken line shows the corresponding results for $E = 37$ dyn cm^{-1} and $\sigma = 34$ dyn cm^{-1}.

8. Discussion and concluding remarks

The compound matrix method seems to be well suited for studying the air–sea interaction problem of the initially growing waves. It has been demonstrated that the growth rate figures calculated with the use of a standard log–linear profile are more or less identical to the numerical results obtained by Creamer & Writer (1992) with the use of a Ricatti method and the same wind profile. The sensitivity of the model to different wind velocity profiles has been tested by comparing the results from three specific choices for the wind distribution. The outcome confirms that the growth of waves in the capillary–gravity regime is not strongly dependent on the exact shape of the velocity profile outside the viscous boundary layer. This is in contradiction to the results reported by Wheless & Csanady (1993), who obtained results with the same numerical method which are almost four times larger than the results obtained here. For waves which have their critical point inside the viscous boundary layer, it has been a usual assumption that the instability is a result of the dynamics of this layer. If this is so, it seems reasonable to expect that small details of the behaviour of the wind velocity profile in the logarithmic region are of minor importance for such waves.

One problem which arises when the turbulent Reynolds stresses are introduced is how to distinguish between the periodic motion induced by the waves, and the fluctuations due to turbulence. If the periods of these two phenomena are of the same order of magnitude, it will in practice be impossible to separate the wave-induced motion from the turbulent fluctuations. To deal with this problem the periods of the waves are assumed to be much longer than the typical time scale of the turbulent

fluctuations. When judging the results presented here for the highest wavenumbers when a turbulent Reynolds stress is included, this problem should be kept in mind.

A somewhat surprising result was that the inclusion of a variable eddy viscosity in the air to some extent reduced the wave growth. In the analytical studies by Jacobs (1987) and by van Duin & Janssen (1992) it was demonstrated that instability might be caused by a positive gradient of the eddy viscosity. One cause for this disagreement might be the simplifications which had to be introduced to be able to find analytical solutions of the equations, but at present more investigations need to be carried out before any definite conclusions about the effect of a variable eddy viscosity on growing waves can be drawn.

The flux of energy from the air to the sea was calculated from the stress perturbation at the surface. The interesting result here was that the latter part had a strong dependence on the elasticity of the surface film. Such a Marangoni effect on the rate of work done by the external forces has not been reported. Just like the Marangoni effect on the dissipation of wave energy, the flux term attains a maximum for a finite value of the film elasticity. The maximum of the dissipation rate appears when the frequencies of the longitudinal film wave and the transverse capillary–gravity wave coincide. The maximum of the flux does not seem to have any such simple relation to the Marangoni wave. When studying how a surface film changes the wave spectrum of the ocean, this effect should probably be taken into account.

A comparison with the measurements of Larson & Wright (1975) and Gottifredi & Jameson (1970) confirms that the present model adequately describes the linear stability of an air–sea interface initially at rest, both for a clean surface and when the surface is contaminated with a surface film. This seems also to be the case for the highest wind speed reported by Larson & Wright if the friction velocity is calculated from a channel-flow profile, using the dimensions on the actual wave tank, instead from a pure logarithmic profile. Since the wind, generated by a fan in a wind tunnel, must attain a maximum near the centre of the tunnel, a channel-flow profile such as the one suggested by Quarmby & Anand will probably give a better description of the actual air flow in this problem than a logarithmic distribution.

Although extensive measurement of film effects on waves have been carried out by several authors, very little seems to have been done on the problem of initially growing waves. The similarity between the numerical results and results obtained by Larson & Wright (1975) and Gottifredi & Jameson (1970) are encouraging with respect to verification of the theoretical model.

This research was supported by The Research Council of Norway under Grant No. 100154/410 through a Research Fellowship. I wish to thank Professor Jan Erik Weber for continuous support and guidance throughout this study. I also wish to thank Professor Kristian Dysthe for introducing me to the laboratory studies of Gottifredi & Jameson, and Professor Arnold Berthelsen for making me aware of the works on turbulent Reynolds stresses by Quarmby & Anand.

Appendix. Compound matrix method

To solve the problem numerically, we formulate the differential equation as a system of first-order equations. It is convenient to write the solution in air and water as linear combinations of the viscous and inviscid parts of the solutions

$$_a = K_1 \ _{1a} + K_2 \ _{2a}, \qquad _w = K_3 \ _{1w} + K_4 \ _{2w}, \tag{A 1}$$

where K_i are undermined constants. To avoid numerical growth caused by the rapidly varying viscous solution a new set of variables is defined as

$$\left.\begin{aligned} y_1 &= \quad _1 \quad _2' - \quad _1' \quad _2, \qquad y_4 = \quad _1' \quad _2'' - \quad _1'' \quad _2', \\ y_2 &= \quad _1 \quad _2'' - \quad _1'' \quad _2, \qquad y_5 = \quad _1' \quad _2''' - \quad _1''' \quad _2', \\ y_3 &= \quad _1 \quad _2''' - \quad _1''' \quad _2, \qquad y_6 = \quad _1'' \quad _2''' - \quad _1''' \quad _2''. \end{aligned}\right\} \tag{A 2}$$

When these are substituted into the differential equation, it can be solved numerically with the use of a standard shooting technique. The problem is then regarded as an initial value problem, and may be integrated with a fourth-order Runga–Kutta method. Far from the surface, an analytic outer solution is found (for details see Wheless & Csanady).

Drazin & Reid (1981, p. 313) give a general set of boundary conditions expressed in terms of the new variables for one medium. For problems involving a coupled system of two media over a wavy interface, Wheless & Csanady (1993) calculated the boundary condition for the new variables for their particular choice of boundary condition with no surface elasticity. Now a general expression for the eigenvalue relation will be outlined, valid for any set of linear boundary conditions between two coupled media.

Four linear boundary conditions may be expressed as

$$\sum_{j=1}^{4} q_{ij}^{a} \quad _{a}^{(j-1)} + \sum_{j=1}^{4} q_{ij}^{w} \quad _{w}^{(j-1)} = 0 \quad \text{for} \quad i = 1, 4, \tag{A 3}$$

where $^{(j-1)}$) means the $j-1$ derivative of with respect to z. A new $4\times$ matrix $\boldsymbol{Q}$, with the following elements may then be constructed:

$$Q_{ij} = \sum_{n=1}^{4} q_{in}^{a} \quad _{ja}^{(n-1)} \quad \text{for} \quad j = 1, 2, \tag{A 4}$$

$$Q_{ij} = \sum_{n=1}^{4} q_{in}^{w} \quad _{j-2w}^{(n-1)} \quad \text{for} \quad j = 3, 4, \tag{A 5}$$

where the subdivision (A 1) for has been introduced. The boundary conditions now yield

$$\operatorname{Det} \boldsymbol{Q} = 0. \tag{A 6}$$

When calculating this determinant by cofactor expansion the new variables will appear. Then the resulting eigenvalue relation may then be expressed in terms of the new variables as

$$A_{12}^{a} A_{34}^{w} + A_{13}^{a} A_{42}^{w} + A_{14}^{a} A_{23}^{w} + A_{23}^{a} A_{14}^{w} + A_{42}^{a} A_{13}^{w} + A_{34}^{a} A_{12}^{w} = 0, \tag{A 7}$$

where

$$\begin{aligned} A_{ij} = {} & (q_{i1} q_{j2} - q_{i2} q_{j1}) y_1 + (q_{i1} q_{j3} - q_{i3} q_{j1}) y_2 + (q_{i1} q_{j4} - q_{i4} q_{j1}) y_3 \\ & + (q_{i2} q_{j3} - q_{i3} q_{j2}) y_4 + (q_{i2} q_{j4} - q_{i4} q_{j2}) y_5 + (q_{i3} q_{j4} - q_{i4} q_{j3}) y_6. \end{aligned} \tag{A 8}$$

Here the subscripts a and w have been deleted since this formula is used for calculating the coefficient A in both air and water.

Following Ng & Reid (1979) the coefficients K_1 and K_2 may be eliminated in four different ways:

$$y_1 \quad '' - y_2 \quad ' + y_4 \quad = 0, \tag{A 9}$$

$$y_1 \quad ''' - y_3 \quad ' + y_5 \quad = 0, \tag{A 10}$$

$$y_2 \quad ''' - y_3 \quad '' + y_6 \quad = 0, \tag{A 11}$$

$$y_4 \quad ''' - y_5 \quad '' + y_6 \quad ' = 0. \tag{A 12}$$

To calculate the eigenfunctions from backward integration of for instance (A 9), the eigenfunction and the first derivative at the boundary must be known. Using a standard technique in linear algebra it is straightforward to show that only two of the equations (A 9)–(A 12) are linearly independent. Accordingly, we need additional information from the boundary conditions. Writing $_a = _w = _o$ and using (A 9) and (A 10) to eliminate $'''$ and $''$ in both air and water, the boundary conditions can be written as

$$\begin{bmatrix} 1 & -1 & A \\ B & C & D \\ E & F & G \end{bmatrix} \begin{bmatrix} {}'_a \\ {}'_w \\ {}_o \end{bmatrix} = 0, \tag{A 13}$$

where the coefficients must be calculated from the boundary conditions (16)–(18), and substituting $'' = (y_2/y_1)\ '-(y_4/y_1)$ and $''' = (y_3/y_1)\ '-(y_5/y_1)$. Gaussian elimination of (A 13) now yields

$${}'_w = \frac{D-AB}{B+C}\ {}_o, \tag{A 14}$$

$${}'_a = {}'_w + A\ {}_o \tag{A 15}$$

subject to the constraint

$$G(C+B)-F(D+E)+A(BF-CE) = 0. \tag{A 16}$$

Finally, the kinematic condition, $\mathrm{D}\zeta/\mathrm{d}t = w$ can be used to express $_o$ in terms of an arbitrary amplitude. In the linear case this is

$$_o = (c-U_o)\,\zeta_o. \tag{A 17}$$

REFERENCES

Alpers, W. & Hühnerfuss, H. 1989 The damping of ocean waves by surface films. a new look at an old problem. *J. Geophys. Res.* **94**, 6251–6265.

Benjamin, T. B. 1958 Shearing flow over a wavy boundary. *J. Fluid Mech.* **6**, 161–205.

Creamer, D. B. & Wright, J. A. 1992 Surface films and wind wave growth. *J. Geophys. Res.* **97**, 5221–5229.

Davey, A. 1979 On the removal of the singularities from the Riccati method. *J. Comput. Phys.* **30**, 137–144.

Donelan, M. A. & Pierson, W. J. 1987 Radar scattering and equilibrium ranges in wind-generated waves with application to scatterometry. *J. Geophys. Res.* **92**, 4971–5029.

Dorrestein, R. 1951 General linearized theory of the effect of surface films on water ripples. *Proc. K. Ned. Akad. Wet.* B*: Palaeontol. Geol. Phys. Chem. Anthropol.* **54**, 260–272, 350–356.

Drazin, P. G. & Reid, W. H. 1981 *Hydrodynamic Stability*. Cambridge University Press.

Duin, C. A. van & Janssen, P. A. E. M. 1992 An analytic model of the generation of surface waves by turbulent air flow. *J. Fluid Mech.* **236**, 197–215.

Dysthe, K. & Rabin, Y. 1986 Damping of short waves by insoluble surface films. In *ONRL Workshop Proc.: the Role of Surfactant Films on the Interfacial Properties of the Sea Surface* (ed. F. L. Herr & J. Williams), pp. 187–213. US Office of Naval Research.

Gastel, K. van, Janssen, P. A. E. M. & Komen, J. 1985 On phase velocity and growth rate of wind-induced gravity–capillary waves. *J. Fluid Mech.* **161**, 199–216.

Gottifredi, J. C. & Jameson, G. J. 1970 The growth of short waves on liquid surfaces under the action of a wind. *Proc. R. Soc. Lond.* A **319**, 373–397.

Herr, F. L. & Williams, J. (Eds.) 1986 *ONRL Workshop Proc.: Role of Surfactant Films on the Interfacial Properties of the Sea Surfaces*. US Office of Naval Research.

Hühnerfuss, H., Lange, P. A. & Walter, W. 1985 Relaxation effects in monolayers and their contribution to water wave damping, part II. *J. Colloid Interface Sci.* **108**, 442–450.

JACOBS, S. J. 1987 An asymptotic theory for turbulent flow over a progressive water wave. *J. Fluid Mech.* **174**, 69–80.

KAWAI, S. 1979 Generation of initial wavelets by instability of a coupled shear flow and their evolution to wind waves. *J. Fluid Mech.* **93**, 661–703.

LAMB, H. *Hydrodynamics*, 6th ed. Cambridge University Press.

LARSON, T. R. & WRIGHT, J. W. 1975 Wind-generated gravity–capillary waves: laboratory measurements of temporal growth rates using microwave backscatter. *J. Fluid Mech.* **70**, 417–436.

LUCASSEN, J. 1982 Effect of surface-active material on the damping of gravity waves: a reappraisal. *J. Colloid Interface Sci.* **85**, 52–58.

MILES, J. W. 1957*a* On the generation of surface waves by shear flows. *J. Fluid Mech.* **3**, 185–204.

MILES, J. W. 1957*b* On the velocity profile for turbulent flow near a smooth wall. *J. Aero. Sci.* **24**, 704.

MILES, J. W. 1962 On the generation of surface waves by shear flows. Part 4. *J. Fluid Mech.* **13**, 433–438.

MILES, J. W. 1993 Surface–wave generation revisited. *J. Fluid Mech.* **256**, 427–441.

NG, B. S. & REID, W. H. 1979 An initial value method for eigenvalue problems using compound matrices. *J. Comput. Phys.* **30**, 125–136.

PHILLIPS, O. M. 1977 *The Dynamics of the Upper Ocean.* Cambridge University Press.

PLUTARCH 95 AD *Historia Naturalis*, book 2, chapter 106.

QUARMBY, A. & ANAND, R. K. 1969 Axisymmetric turbulent mass transfer in a circular tube. *J. Fluid Mech.* **38**, 433–455.

SCOTT, J. C. 1977 The historical development of theories of wave-calming using oil. *Hist. Technol.* **3**, 163–186.

WEBER, J. E. & SAETRA. Ø. 1995 Effect of film elasticity on the drift velocity of capillary–gravity waves. *Phys. Fluids* **7**, 307–314.

WHELESS, G. H. & CSANADY, G. T. 1993 Instability waves on the air–sea interface. *J. Fluid Mech.* **248**, 363–381.